Fine-tuning the metallic core-shell nanostructures for plasmonic perovskite solar cells

Mingyao Tang, Lin Zhou, Shuai Gu, Weidong Zhu, Yang Wang, Jun Xu, Zhengtao Deng, Tao Yu, Zhenda Lu, and Jia Zhu

Citation: Appl. Phys. Lett. **109**, 183901 (2016); doi: 10.1063/1.4966893
View online: https://doi.org/10.1063/1.4966893
View Table of Contents: http://aip.scitation.org/toc/apl/109/18
Published by the American Institute of Physics

Fine-tuning the metallic core-shell nanostructures for plasmonic perovskite solar cells

Mingyao Tang,[1,a)] Lin Zhou,[1,a)] Shuai Gu,[1] Weidong Zhu,[2] Yang Wang,[1] Jun Xu,[3] Zhengtao Deng,[1] Tao Yu,[2] Zhenda Lu,[1,b)] and Jia Zhu[1,b)]
[1]*National Laboratory of Solid State Microstructures, College of Engineering and Applied Sciences, and Collaborative Innovation Center of Advanced Microstructures, Nanjing University, Nanjing 210093, China*
[2]*National Laboratory of Solid State Microstructures and Eco-Materials and Renewable Energy Research Center (ERERC), Department of Physics, Nanjing University, Nanjing 210093, China*
[3]*National Laboratory of Solid State Microstructures and School of Electronic Science and Engineering, Nanjing University, Nanjing 210093, China*

(Received 31 August 2016; accepted 19 October 2016; published online 1 November 2016)

Plasmonic nanostructures have been widely applied in various types of solar cells for improving light absorption and therefore energy conversion efficiency. In this work, we demonstrate that Au@SiO_2 core-shell nanorods with finely tuned aspect ratios are highly beneficial for the $CH_3NH_3PbI_3$ perovskite solar cell, with the simultaneous enhancement of solar absorption and external quantum efficiency across a broad range of wavelength, which can contribute to the increased cross-sectional scattering and spectrally absorbing energy density. Therefore, a 16.1% improvement (from 12.4% to 14.4%) of the maximal external quantum efficiency can be achieved by such structures, accompanied with a 13.5% improvement (from 20.0 to 22.7 mA/cm^2) of the maximal short-circuit current density and little improvement of the open-circuit voltage and fill factor. Our findings also provide a general guideline to design solar cell structures with thinner absorber layers and improve the absorption in other poorly light-absorbing devices like lead free perovskite solar cells as well. *Published by AIP Publishing.* [http://dx.doi.org/10.1063/1.4966893]

The field of plasmonics has drawn extensive interests because of its unique abilities of guiding and localizing light at the subwavelength scale, showing potential applications for a wide range of solar energy conversion systems such as photovoltaics,[1,2] solar-thermal[3–6] solar-to-chemistry energy conversions,[7–9] etc. It is clear that the metallic nanostructures located at different positions in plasmonic photovoltaic cells can play different roles.[1,10,11] In the past decades, these plasmon-enhanced light trapping mechanisms have been widely employed in various types of solar cells ranging from inorganic (like single-crystalline Si, amorphous Si, GaAs and quantum well)[12–15] to organic (including dye-sensitized)[16–20] solar cells. Most recently, several research groups tried to reveal the localized surface plasmon resonance (LSPR) effect in the metal nanoparticles (NPs)-incorporated organic–inorganic halide perovskite solar cells (PSCs)[21–25] without conclusive explanations.[26,27] There are rigorous requirements to enable pronounced absorption enhancement. For example, metallic gratings at the rear side require precise momentum matching with rigorous periodicity designs, which are commonly narrow-band. Metallic nanoparticles (NPs) on the top surface encounter tradeoff between backward scattering (and/or surface reflection) and the intrinsic ohmic loss of metals. Metallic NPs embedded inside active materials may deteriorate the interface of p-n junction and therefore the electron transport. In this work, by fine-tuning the structures and scattering characteristics of Au@SiO_2 core-shell nanorods (NRs), we report the pronounced plasmonic enhanced perovskite solar cells with 16.1% improvement in the maximal (8.3% in averaged) photo-to-current efficiency (PCE) of PSC doped with Au@SiO_2 NRs, accompanied with the broadband distinct absorption and external quantum efficiency (EQE) enhancement.

Since the shape and size of the plasmonic NPs are crucial for plasmonic absorption enhancement,[28] it should be spectrally optimized according to the absorption spectrum of the $CH_3NH_3PbI_3$ perovskite film for demonstrating the plasmon-enhanced effect. There are typically several factors for the design of plasmon-mediated perovskite absorber. (1) Plasmonic near field enhancement, the most well-known plasmon-mediated method, can be effective provided that the active material is located in extremely close proximity of the metallic NPs ($\sim$<10 nm),[24,29] which is commonly impactful around the LSPR wavelength. (2) Strong plasmon-induced light scattering effect would be dominant if the metallic NPs have large scattering cross sections, which can contribute to broadband absorption enhancement because of the increased optical absorption path length inside the perovskite materials.[20,30] (3) The LSPR wavelength of the NPs should be easy to tune. In addition, because of relatively poor absorption performance around band edge of the active absorbing materials, NPs with LSPR wavelength tuned around the band edge of the perovskite (for example, $CH_3NH_3PbI_3$ $\sim$700 to 780 nm) would be more preferred. (4) The metallic-insulating core-shell structures are most widely employed because the insulating shell can effectively prevent direct conduction between plasmonic metals and hole transport layer (HTL) or perovskite so that unwanted recombination pathway can be prohibited. In this work, we demonstrate that the real useful and broadband absorption enhancement, which can directly contribute to enhanced short-circuit current, is coming

[a)]M. Tang and L. Zhou contributed equally to this work.
[b)]Electronic addresses: jiazhu@nju.edu.cn and luzhenda@nju.edu.cn

from the plasmonic scattering effect. Based on the above considerations together with the flexible tunability of the LSPR, $Au@SiO_2$ NR is chosen as the doping NP. Furthermore, in order to achieve maximized absorption performance of perovskite material by plasmonic scattering enhancement, $Au@SiO_2$ NR with the aspect ratio ($AR = L/D$) of the metallic core (~3) and thickness of the insulating shell ($t \sim 15$ nm) is finally chosen based on the systematic calculations (Figure 2(a), supplementary material, S I, Figures S1–S5).

The only difference between the standard and doped PSCs is whether there are $Au@SiO_2$ NRs in the mesoporous layer. The standard PSCs are the reference cells, while the doped PSCs represent the $Au@SiO_2$ NRs incorporated PSCs. The schematic diagram of the $Au@SiO_2$ doped active layer is shown in Figure 1(a), which is a typical thin film profile in the form of FTO/electron transport layer (ETL)/absorbing layer/hole transport layer (HTL)/Au electrode. TiO_2 compact film and spiro-OMeTAD film served as the ETL and HTL, respectively. The absorbing layer of the doped PSC is an $Au@SiO_2$ nanorod assembly embedded in the $CH_3NH_3PbI_3$ perovskite film, which is composed of a small amount of $Au@SiO_2$ core-shell NRs and large amount of small TiO_2 NPs, without distinct influence on the uniformity (supplementary material, Figure S6), while the standard PSC (without doping $Au@SiO_2$ NRs) served as the reference cell throughout the following discussion of the manuscript. The $Au@SiO_2$ core-shell NRs are synthesized based on the standard solution-based method in the literature, a representative TEM image of which is shown Figure 1(b). The UV-Vis absorbance spectrum (Figure 1(c)) reveals that the LSPR wavelength of the as-prepared $Au@SiO_2$ core-shell nanorods (inside ethanol solution) is ~735 nm, which would be red-shifted by several tens of nanometers (closer to the band edge of $CH_3NH_3PbI_3$) with the background material changed to the higher indexed active layer (supplementary material, Figure S1). Meanwhile, the shape and size of the prepared $Au@SiO_2$ NRs could achieve high scattering efficiency as well as broad LSPR wavelength.

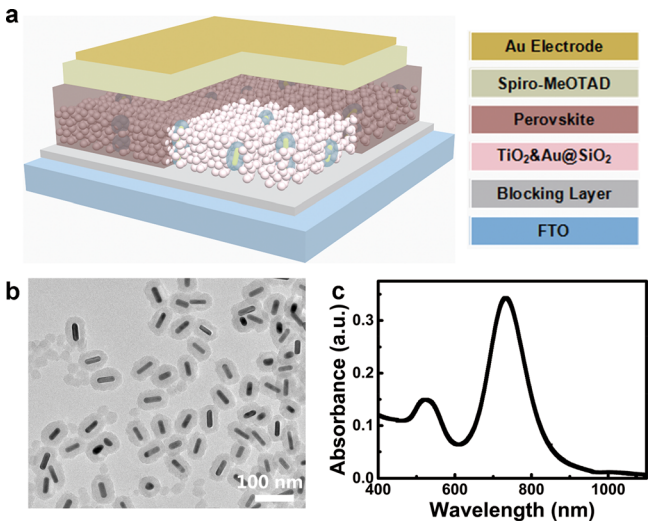

FIG. 1. (a) Schematic diagram of the $Au@SiO_2$ core-shell nanorods doped perovskite solar cells. (b) TEM image of the as-prepared $Au@SiO_2$ core-shell nanorods. The scale bar stands for 100 nm. (c) Measured UV-Vis absorbance spectrum of the $Au@SiO_2$ nanorods dispersed in ethanol solution.

We first demonstrate the enhanced scattering effect of the $Au@SiO_2$ NRs. Taking the typical $Au@SiO_2$ core-shell NR (the average size of the doped sample: AR~3, shell thickness ~15 nm) for example (supplementary material, Figure S8), the only geometry difference between the doped and standard PSC is that a certain number of close-packed TiO_2 nanosphere (the average diameter ~22 nm) clusters are replaced by $Au@SiO_2$ NRs, as shown in Figure 2(a). Without the loss of generality, a single representative $Au@SiO_2$ NR (the geometry parameters of the most dominant NRs in Figure 1(b) are employed) and the equivalent TiO_2 nanosphere cluster (with almost equivalent volume and projected geometry cross-

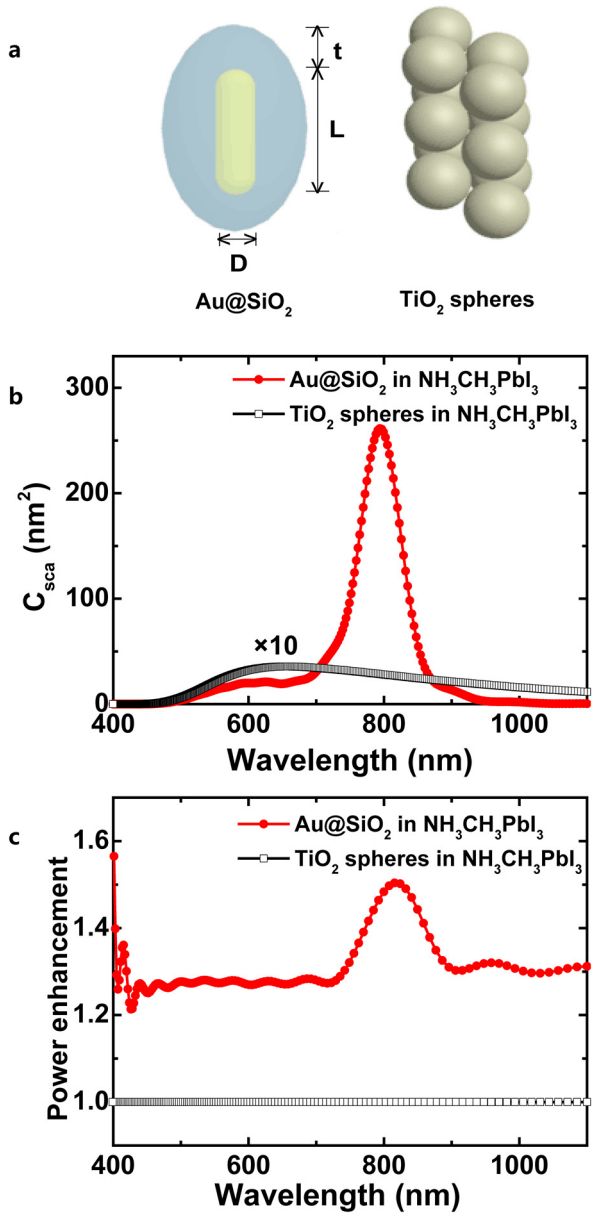

FIG. 2. (a) Optical modeling of the $Au@SiO_2$ core-shell nanorod and the substituted TiO_2 nanosphere cluster. The aspect ratio (L/D) of the Au rod is ~3 and the SiO_2 shell thickness (t) is ~15 nm. The diameter of the TiO_2 nanosphere is 22 nm. (b) FDTD calculated scattering cross-section C_{sca} of the two geometries (in (a)) embedded inside the perovskite materials: red circles for the $Au@SiO_2$ and black square for TiO_2 cluster. The absolute C_{sca} of TiO_2 geometry is multiplied by 10 for clear comparison. (c) Calculated spectral dependence of the integrated power enhancement (respect to the standard geometry of TiO_2 spheres) inside perovskite materials in a 100 nm × 100 nm × 100 nm unit cell.

section area) are considered. Three dimensional full wave electromagnetic simulations based on the finite difference time domain (FDTD) method are performed in order to reveal how the scattering effect enhances the optical absorption of perovskite (supplementary material, S I). The calculated scattering cross-sections C_{sca} of the two target geometries (Figure 2(a)) are shown in Figure 2(b). One can strikingly observe that the light scattering performance can be increased by two orders of magnitude at the resonant wavelength of the LSP mode of the Au@SiO_2NR, which is still several times larger than the referenced TiO_2 nanosphere cluster even far away from the resonant wavelength range. Such strong light scattering enhancement around the band edge of $CH_3NH_3PbI_3$ can distinctly improve the absorption performance. In order to estimate whether the doped Au@SiO_2 NR can produce an perovskite absorption enhancement or not, we calculate the spectral power enhancement in the one Au@SiO_2 NR doped active layer (relative to the standard active layer) by integrating the power inside perovskite materials in a 100 nm × 100 nm × 100 nm volume, as shown in Figure 2(c). The plot shows a pronounced absorbing power enhancement in the range of 750–850 nm (around the LSP wavelength of Au@SiO_2 embedded in perovskite). In addition, the entire increment of power enhancement in Figure 2(c) indicates that the overall absorption of perovskite material can be improved by >20% across the entire visible to infrared region. Furthermore, a more precise FDTD simulation based on the modeling of the real 3D morphology is performed, in which the doping concentration is closer to the experimental case. Then, the total absorption spectrum as well as absorption power of perovskite film (the thickness ~400 nm, the transverse period ~400 nm × 400 nm) is calculated (supplementary material, Figures S4 and S5). One can clearly observe the broadband absorption enhancement (400–800 nm) instead of merely distinct enhancement around the LSPR wavelength. Therefore, it is clear that the absorption enhancement can be ascribed to the plasmonic scattering effect instead of plasmonic near field enhancement (supplementary material, S II).

To demonstrate the plasmon-enhanced solar absorption enhancement of the doped PSC, we tested the experimental absorption performance as well as the EQE of the solar cells. Figure 3(a) shows a typical cross-sectional SEM image of the Au@SiO_2 NRs doped PSC with the doped absorbing layer enlarged in Figure 3(b). The unchanged overall thickness and the flat interface of perovskite and HTL indicate that the overall quantity of active material in the doped PSC is approximately equivalent to that of the standard PSC. The total absorption spectra of the doped and standard active layers (on the compact TiO_2/FTO substrate) were measured by the integrating sphere UV-Vis system, as shown in Figure 3(c). It means that the absorption efficiency of the active layer (with the same substrate) can be indeed broadband improved, which reaches the maximal around the band edge of $CH_3NH_3PbI_3$ material (agreed well with the calculated power enhancement in Figure 2(c)). One can find that the EQE performance of the doped PSC is also broadband enhanced, as shown in Figure 3(d), indicating that most of the enhanced solar absorption can be converted into effective electron-hole pairs.

The validity evaluation of our photon management on the performance of the PSC devices is then carried out by

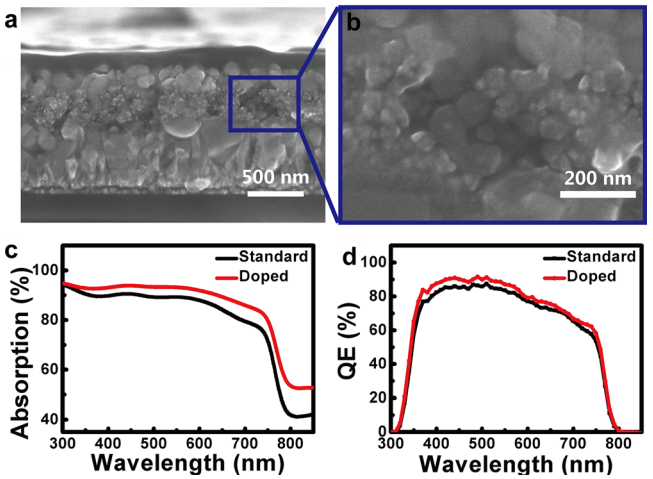

FIG. 3. (a) and (b) Representative cross-sectional SEM images of the Au@SiO_2 nanorods doped perovskite solar cell with locally amplified in (b). (c) and (d) Measured (c) absorption efficiency and (d) quantum efficiency (QE) curves of the Au@SiO_2 doped (red circles) and standard (black squares) perovskite films on the same TiO_2/FTO substrates, respectively.

the electrical characterizations. Figure 4 shows the most representative photocurrent density-voltage (J-V) curves of the doped and standard PSC devices with the same active layer thickness (~400 nm). The scan direction of the cell performance presented was from the forward bias (FB) to the short circuit (SC). Both of the doped and standard cells had the hysteresis effect (supplementary material, Figure S7). The standard PSC has a peak PCE of 12.4%, while the Au@SiO_2 doped PSC exhibits a PCE of 14.4% (16.1% higher than the standard device). Compared with the standard device, the fill factor (*FF*) and open-circuit voltage (V_{oc}) are similar, while the short-circuit current density (J_{sc}) significantly increased from 20.0 to 22.7 mA/cm^2. To ensure the reliability, we fabricated 30 sets of PSC devices with (the doping concentration ~4 wt. %) and without Au@SiO_2 NRs, respectively (supplementary material, S V).

Figure 5 shows the statistic distributions of the J_{sc}, V_{oc}, *FF* and *PCE* of 30 sets of devices, with the average device performance parameters listed in Table I. One may find that an

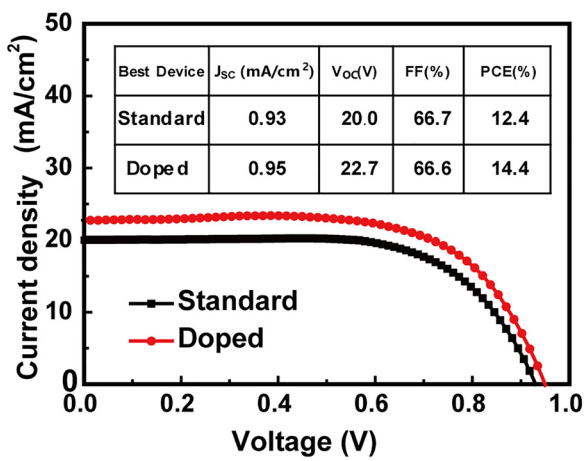

FIG. 4. Representative J−V curves for the Au@SiO_2 nanorods doped (red circles) and standard (black squares) devices measured under the AM1.5 simulated sunlight (100 mW/cm^2 irradiance). The detailed photovoltaic parameters of the two devices are shown in the inset.

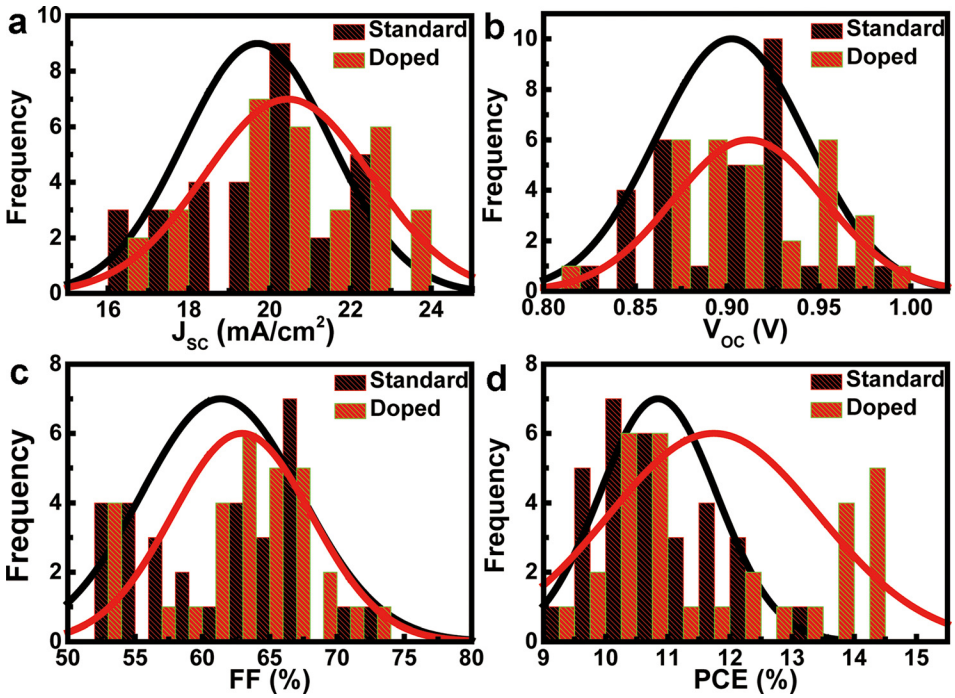

FIG. 5. The statistic distribution of (a) short-circuit current density J_{sc}, (b) open-circuit voltage V_{oc}, (c) fill factor FF, and (d) power conversion efficiency PCE for 30 doped and standard devices, respectively. The bottom table shows the direct comparison of the average performance of the doped and standard devices.

TABLE I. Average photovoltaic parameters of the Au@SiO_2 doped PSC and standard PSC devices as measured over 30 devices.

Device	J_{sc} [mA/cm^2]	V_{oc} [V]	FF	PCE [%]
Au@SiO_2 doped	20.5	0.91	0.63	11.7
Standard	19.7	0.90	0.61	10.8

average PCE of 11.7% was achieved by the Au@SiO_2 doped device, which is 8.4% higher than the average standard device efficiency of 10.8%. The distinct PCE improvement is accompanied with the average J_{sc} increased by 4.1% from 19.7 to 20.5 mA/cm^2, which originates from the broadband absorption enhancement that has been demonstrated both by the experimental absorption as well as EQE measurements (Figures 3(c) and 3(d)) and by the numerical calculations of scattering induced broadband absorbing power increment (Figures 2(b) and 2(c)). The less pronounced enhancement of EQE around the band edge may be related to the intrinsic metal absorption (supplementary material, S II). In the meantime, the average V_{oc} only slightly increased from 0.90 V to 0.91 V and average FF slightly increased from 0.61 to 0.63, which may be related to the better morphology control of the doped perovskite film. Therefore, we are safe to conclude that the incorporation of Au@SiO_2 NRs has improved the device performance mainly by enhancing the photocurrent directly via the plasmonic scattering enhanced broadband absorption.

In conclusion, we have demonstrated the plasmonic perovskite thin film solar cells by incorporating the Au@SiO_2 core-shell nanorods with fine-tuned geometry into the $CH_3NH_3PbI_3$/mesoporous TiO_2 active layer. By precise design of the plasmon-enhanced scattering performance of the Au@SiO_2 nanorods, the absorption efficiency of the perovskite can be broadband enhanced, which can contribute to the broadband EQE and integrated J_{sc} increment. In addition, the doping procedure is well compatible with the solution-based fabrication processes of the perovskite solar cell; thus, the electric performance of the doped PSC is also well maintained. As a result, a maximal PCE of up to 14.4% is achieved (~16.1% higher than that of the standard device). Because of the broadband enhancement feature as well as the less confinement on the precise geometry control, such scattering manipulation strategy is much easier to extend to thin film solar cells compared with the traditional plasmonic enhanced effect, such as the near-field E field enhancement and/or multiple plasmonic mode excitations, etc. Our results provide a complementary strategy for broadband plasmonic enhancement as well as a clear understanding on the mechanism of metallic-nanoparticle-mediated perovskite solar cells.

See supplementary material for the optimization of the size of Au@SiO_2 NRs. We calculated the full wave simulation of the absorption spectra of standard and four Au@SiO_2 NRs doped mesoporous-TiO_2-perovskite film with different AR and integrated power inside perovskite materials for standard geometry and four Au@SiO_2 NRs doped film, respectively. Meanwhile, the details of device fabrication, optical modeling and numerical simulation were also presented.

This work is jointly supported by the State Key Program for Basic Research of China (No. 2015CB659300), the National Natural Science Foundation of China (Nos. 11321063 and 11574143), and the Natural Science Foundation of Jiangsu Province (Nos. BK20150056 and BK20151079).

[1]H. A. Atwater and A. Polman, Nat. Mater. **9**, 205 (2010).
[2]R. A. Pala, J. White, E. Barnard, J. Liu, and M. L. Brongersma, Adv. Mater. **21**, 3504 (2009).
[3]L. Zhou, Y. Tan, J. Wang, W. Xu, Y. Yuan, W. Cai, S. Zhu, and J. Zhu, Nat. Photonics **10**, 393 (2016).
[4]K. Bae, G. Kang, S. K. Cho, W. Park, K. Kim, and W. J. Padilla, Nat. Commun. **6**, 10103 (2015).
[5]L. Zhou, Y. Tan, D. Ji, B. Zhu, P. Zhang, J. Xu, Q. Gan, Z. Yu, and J. Zhu, Sci. Adv. **2**, e1501227 (2016).
[6]L. Zhou, X. Yu, and J. Zhu, Nano Lett. **14**, 1093 (2014).

[7]S. Linic, P. Christopher, and D. B. Ingram, Nat. Mater. **10**, 911 (2011).
[8]S. Mubeen, J. Lee, N. Singh, S. Kramer, G. D. Stucky, and M. Moskovits, Nat. Nanotechnol. **8**, 247 (2013).
[9]S. C. Warren and E. Thimsen, Energy Environ. Sci. **5**, 5133 (2012).
[10]V. E. Ferry, L. A. Sweatlock, D. Pacifici, and H. A. Atwater, Nano Lett. **8**, 4391 (2008).
[11]K. R. Catchpole and A. Polman, Opt. Express **16**, 21793 (2008).
[12]D. M. Schaadt, B. Feng, and E. T. Yu, Appl. Phys. Lett. **86**, 063106 (2005).
[13]D. Derkacs, S. H. Lim, P. Matheu, W. Mar, and E. T. Yu, Appl. Phys. Lett. **89**, 093103 (2006).
[14]K. Nakayama, K. Tanabe, and H. A. Atwater, Appl. Phys. Lett. **93**, 121904 (2008).
[15]D. Derkacs, W. V. Chen, P. M. Matheu, S. H. Lim, P. K. L. Yu, and E. T. Yu, Appl. Phys. Lett. **93**, 091107 (2008).
[16]A. J. Morfa, K. L. Rowlen, T. H. Reilly, M. J. Romero, and J. van de Lagemaat, Appl. Phys. Lett. **92**, 013504 (2008).
[17]L. Lu, Z. Luo, T. Xu, and L. Yu, Nano Lett. **13**, 59 (2013).
[18]J. Yang, J. You, C. C. Chen, W. C. Hsu, H. R. Tan, X. W. Zhang, Z. Hong, and Y. Yang, ACS Nano **5**, 6210 (2011).
[19]M. D. Brown, T. Suteewong, R. S. S. Kumar, V. D'Innocenzo, A. Petrozza, M. M. Lee, U. Wiesner, and H. J. Snaith, Nano Lett. **11**, 438 (2011).
[20]I. K. Ding, J. Zhu, W. Cai, S. J. Moon, N. Cai, P. Wang, S. M. Zakeeruddin, M. Grätzel, M. L. Brongersma, Y. Cui, and M. D. McGehee, Adv. Energy Mater. **1**, 52 (2011).
[21]A. Kojima, K. Teshima, Y. Shirai, and T. Miyasaka, J. Am. Chem. Soc. **131**, 6050 (2009).
[22]M. M. Lee, J. Teuscher, T. Miyasaka, T. N. Murakami, and H. J. Snaith, Science **338**, 643 (2012).
[23]H. S. Kim, C. R. Lee, J. H. Im, K. B. Lee, T. Moehl, A. Marchioro, S. J. Moon, R. Humphry-Baker, J. H. Yum, J. E. Moser, M. Grätzel, and N. G. Park, Sci. Rep. **2**, 591 (2012).
[24]J. H. Im, I. H. Jang, N. Pellet, M. Gratzel, and N. G. Park, Nat. Nanotechnol. **9**, 927 (2014).
[25]J. Burschka, N. Pellet, S. J. Moon, R. Humphry-Baker, P. Gao, M. K. Nazeeruddin, and M. Gratzel, Nature **499**, 316 (2013).
[26]W. Zhang, M. Saliba, S. D. Stranks, Y. Sun, X. Shi, U. Wiesner, and H. J. Snaith, Nano Lett. **13**, 4505 (2013).
[27]J. Cui, C. Chen, J. B. Han, K. Cao, W. J. Zhang, Y. Shen, and M. K. Wang, Adv. Sci. **3**, 1500312 (2016).
[28]C. P. Huang, X. G. Yin, H. Huang, and Y. Y. Zhu, Opt. Express **17**, 6407 (2009).
[29]W. L. Liu, F. C. Lin, Y. C. Yang, C. H. Huang, S. Gwo, M. H. Huang, and J. S. Huang, Nanoscale **5**, 7953 (2013).
[30]K. R. Catchpole and A. Polman, Appl. Phys. Lett. **93**, 191113 (2008).